Climate Dynamics (2021) 57:2491–2504
https://doi.org/10.1007/s00382-021-05817-6

Precipitation over Indochina during the monsoon transition: modulation by Indian Ocean and ENSO regimes

Fei Ge[1,4] · Shoupeng Zhu[2,3,4] · Frank Sielmann[5] · Klaus Fraedrich[4] · Xiuhua Zhu[4,5] · Ling Zhang[3] · Xiefei Zhi[3] · Hao Wang[6]

Received: 25 October 2020 / Accepted: 12 May 2021 / Published online: 11 June 2021

Abstract
The interannual variability of precipitation during the summer monsoon transition over the Indochina Peninsula (ICP) is substantially influenced by the sea surface temperature anomalies (SSTAs) of the tropical ocean, showing a robust relationship between April and May (AM) precipitation and the El Niño/Southern Oscillation (ENSO) phenomenon. Dynamic composites and statistical analyses supported by model experiments indicate that the observed anomalous AM precipitation is associated with circulation anomalies over the Pacific and, in addition, affected by the response to the tropical SSTAs forcing from the Indian Ocean (IO): (i) Less (greater) than normal AM precipitation over the ICP occurs during the El Niño (La Niña) years, which is consistent with late (early) Bay of Bengal (BoB) summer monsoon onset. (ii) The dry (wet) AM precipitation years are associated with the anomalous western North Pacific (WNP) anti-cyclone (cyclone) induced by El Niño (La Niña) concurrent with the anti-cyclone (cyclone) over the BoB, suppressing (favoring) the meridional flow of warm and moist air from the Pacific and Indian ocean and thus cutting (providing) moisture supply for the ICP. (iii) The reduced tropical convective activity over Maritime Continent (MC) is related to the weakened local Hadley circulation concurrent with the weakened overturning Walker circulation, and favors a drier than normal AM precipitation over the ICP, to which the wetter years are opposite. These symmetric atmospheric circulation patterns characterizing dry and wet AM precipitation over the ICP are also reproduced by numerical experiments with an atmospheric general circulation model.

Keywords Precipitation · Indochina Peninsula · Monsoon transition · ENSO

1 Introduction

The Indochina Peninsula (ICP), located between the Indian Ocean (IO) and the western Pacific, is strongly affected by the tropical monsoon regime, which dominates weather and climate (Matsumoto 1997; Wang and Fan 1999). The monsoonal precipitation over the ICP has the distinct characteristic of a dry season from October to the subsequent April followed by a rainy season from May to September on which local water resources, food security and crop production are particularly dependent (Wu and Wang 2000; Takahashi and Yasunari 2006; Zhu et al. 2020a). Furthermore, extreme precipitation events in the tropics are also affected by climate change and, therefore, more likely to occur under rapid global warming with increasing frequency of weather and climate extremes disrupting agricultural industries, imposing the heavy drought/flood risks and leading to huge social stresses (Allen and Ingram 2002; Knutson et al. 2010; Zhang et al. 2014; Ge et al. 2021). Thus, the investigation

✉ Shoupeng Zhu
zspshoupeng@163.com

1 School of Atmospheric Sciences/Plateau Atmosphere and Environment Key Laboratory of Sichuan Province/Joint Laboratory of Climate and Environment Change, Chengdu University of Information Technology, Chengdu, China

2 Nanjing Joint Institute for Atmospheric Sciences, Chinese Academy of Meteorological Sciences, Nanjing, China

3 Key Laboratory of Meteorological Disaster, Ministry of Education/Collaborative Innovation Center On Forecast and Evaluation of Meteorological Disasters, Nanjing University of Information Science and Technology, Nanjing, China

4 Max Planck Institute for Meteorology, Hamburg, Germany

5 Meteorological Institute, University of Hamburg, Hamburg, Germany

6 College of Atmospheric Sounding, Chengdu University of Information Technology, Chengdu, China

of interannual variability of precipitation is fundamental to understanding the physical mechanisms, which potentially determine predicting signals several months in advance, supporting countries in and around the ICP to implement effective adaptations.

Plenty of efforts in the past several decades have improved the understanding of the interannual and interdecadal variability of climate in Southeast Asia (He et al. 1987; Matsumoto 1992; Webster et al 1998; Lau et al. 2000; Wang et al. 2001; McBride et al. 2003; Takahashi and Yasunari 2008; Fan et al. 2018; Zhu 2018). Many studies have documented that the rainy season precipitation over the ICP has a significant relationship with ENSO (Zhou et al. 2011; Hsu et al. 2014; Villafuerte and Matsumoto 2015; Ge et al. 2017; Fan et al. 2019). Individual countries, e.g. Vietnam, Thailand and Myanmar, are prone to experiencing temperature and precipitation extremes during the decaying phase of the ENSO life cycle (Manton et al. 2001; Nicholls et al. 2005; Caesar et al. 2011; Nguyen et al.2014; Sein and Zhi 2016). These results indicate that ENSO modulating the interannual variability of summer monsoon precipitation remains an important scientific challenge, and how the spatial scales of South East Asia, the main land at large and the individual countries of the ICP, are affected.

It is generally recognized that the onset of the Asian monsoon initially occurs over the Bay of Bengal (BoB) from late April to early May, establishing strong convective activities and the change of direction of the prevailing wind. A number of studies have shown a connection between increased convection and patchy cells of convective storms over the ICP during the monsoon transition over the Asian continent (Lau and Yang 1997; Wu and Zhang 1998; Zhang et al. 2002; Wang and Chan 2002; Li and Zhang 2009). On the other hand, the rainy season precipitation variability over the ICP is closely related to the early/late BoB summer monsoon (BoBSM) onset (Wang and LinHo 2002; Mao and Wu 2007; He and Zhu 2015; Liu et al 2015). The early/late BoBSM onset is more likely to occur during the La Niña/El Niño years (Wang et al. 2013; Xing et al. 2016; Li et al. 2018). Following these studies, we will refer to the role of convection, represented here by anomalous patterns of outgoing longwave radiation and apparent heat source, in Sect. 3.2.

The rainy season precipitation over the ICP is generally divided into three periods: onset/transition (April–May), peak (June–August) and withdrawal (September–October), which are associated with the summer monsoon activities. However, the interannual variability in precipitation during the rainy season over the ICP has yet not been comprehensively revealed. Many studies have focused on the peak and post-monsoon period, suggesting that precipitation is mainly contributed by tropical cyclones crossing the ICP (Fudeyasu et al. 2006; Takahashi and Yasunari 2008; Takahashi et al. 2015). However, the monsoon transition related precipitation and its variability have seldom been investigated with latest high-resolution observational datasets for the Southeast Asian region. The remote SST forcing over the tropical Pacific associated atmospheric processes may influence year-to-year variabilities of AM precipitation over the ICP. The identification of impact factors triggering the monsoon onset and the assessment of associated precipitation variabilities appear to be crucial for understanding the early intense floods in the ICP region. Thus, there are several issues still open: (1) How are interannual variabilities of AM precipitation linked to ENSO events? (2) How does the atmosphere respond to the tropical SSTAs? In the following sections, we use the latest observations and an ensemble of sensitivity experiments to investigate the relationship between the tropical SST forcing and AM precipitation over the ICP.

This paper is organized as follows. Datasets, methods of analysis and the adopted atmospheric general circulation model (GCM) are introduced in Sect. 2. The interannual variability of precipitation during the monsoon transition over the ICP, referring to April and May (AM), and the possible teleconnections with the tropical Pacific and IO are presented in Sect. 3. Results of the corresponding numerical experiments are shown in Sect. 4. Conclusions and discussions follow in Sect. 5.

2 Data and methods of analysis

2.1 Observations

In this study, the observed monthly mean precipitation and surface air temperatures (SATs) over the ICP (6°N–23°N, 96°E–110°E) for the time period 1981–2016 with a resolution on 0.5° × 0.5° are obtained from the Southeast Asian Climate Assessment and Dataset (SACA&D). This new high- resolution (land-only) dataset, called SA-OBSv2.0, has undergone strict quality control procedures, including data homogenization and time consistency, to improve reliability. Detailed descriptions of this dataset could be found in van den Besselaar et al. (2017).

The National Centers for Environment Prediction/National Center for Atmospheric Research (NCEP/NCAR) reanalysis dataset (Kalnay et al. 1996) are also used in this study. Upper-air variables (e.g.: wind fields, geopotential height and relative humidity) have a spatial resolution of 2.5° × 2.5° with 17 vertical pressure levels. The interpolated Outgoing Longwave Radiation (OLR) data (Liebmann and Smith 1996) are derived from the National Oceanic and Atmospheric Administration (NOAA) with a horizontal resolution of 2.5° × 2.5°. In addition, global monthly mean SST data is from the Extended Reconstructed Sea Surface Temperature dataset (ERSST; Huang et al. 2015; 2017) with a horizontal resolution of 2°×2°. The NCEP/NCAR reanalysis, OLR and ERSST datasets cover the same period as the observations (1981–2016).

The Oceanic Niño Index (ONI), the primary indicator for monitoring El Niño and La Niña events by Climate Prediction Center of the National Oceanic and Atmospheric Administration (NOAA), is considered to represent ENSO variability in this study, which is computed as the 3-month running mean SST anomaly (SSTA) over the Niño 3.4 region (5°N-5°S, 120°-70°W) (Huang et al. 2017). A warm (cold) ENSO event is defined when the winter ONI value is greater (less) than 0.6 °C (– 0.6 °C). The winter and spring in this study are defined as December–January–February (DJF) and March–April–May (MAM), respectively. Note that the number -1 denotes the previous year but not to ENSO cycle.

The empirical orthogonal function (EOF) analysis is employed to capture the dominant modes of AM precipitation variations over the ICP. The composite and linear correlation analyses are applied to investigate the spatial and temporal variability of AM precipitation anomalies and its association with the large-scale SSTAs. The onset dates of the BoBSM (Li et al. 2018) are defined as the areal mean zonal wind at 850 hPa (*U850*) over 90°–100°E, 5°–15°N, satisfying the following two criteria: (1) the day where *U850* exceeds 0 m/s and (2) when the mean *U850* is larger than 2 m/s in the subsequent 10 days (including the onset day).

According to Yanai et al. (1973, 1992) and Yanai and Li (1994), the apparent heat source Q_1 is calculated by

$$Q_1 = C_p\left(\frac{p}{p_0}\right)^k\left[\frac{\partial\theta}{\partial t} + \vec{V}\cdot\nabla\theta + \omega\frac{\partial\theta}{\partial p}\right] = Q_R + L(c-e) - \frac{\partial\left(\overline{s'\omega'}\right)}{\partial p} \quad (1)$$

where θ is the potential temperature, V the horizontal wind, ω the vertical $p-$ velocity, $k = R/C_p$,R and C_p are the gas constant and the specific heat at constant pressure of dry air, L the latent heat, $p_0 = 1000hPa$,Q_R the radiative heating rate, $s = c_pT + gz$ the dry static energy, c the rate of condensation per unit mass of air and e the rate of re-evaporation of cloud and rain water. Statistical significance is examined by a two-tailed Student's t-test. Note that the long-term linear trends in all datasets have been removed.

2.2 Model and model experiments

The intermediate complexity climate model, Planet Simulator (PlaSim; Fraedrich et al. 2005a, b), is used to conduct the numerical experiments to investigate atmospheric circulation and moisture transport responding on different SSTAs forcing during the monsoon transition. PlaSim is a spectral general circulation model (GCM), whose dynamical core is based on Portable University Model of the Atmosphere (PUMA), an atmospheric GCM that solves the moist primitive equations conserving momentum, mass and energy in the Earth's atmosphere. The atmospheric module is coupled to a 5-layer land surface model with biosphere. The ocean is represented by a 50 m depth mixed layer-ocean, which includes a thermodynamic sea-ice model. The horizontal resolution used in this study is T42 (2.8°×2.8°) with 10 vertical sigma levels (for more details see Lunkeit et al. (2011).

The Planet Simulator (PlaSim) is freely available for download at https://www.mi.uni-hamburg.de/en/arbeitsgruppen/theoretische-meteorologie/modelle/plasim.html. It is known in the world-wide user community (including the Open University in England, National Research Council of Italy, Siberian Branch of the Russian Academy of Sciences, and Peking University etc.), this model, being one of the few freely available GCMs, has also been constructed for reproducibility, a demand required for physical experiments in general (Holden et al. 2014). Previous studies have demonstrated that PlaSim can be successfully employed to analyze the evolution of the climate system under different physical scenarios (Bordi et al. 2012, 2013; Holden et al. 2016). It also shows a high skill in reproducing the global impacts of the tropical SST anomalies in an idealized numerical modelling environment (Dahms et al. 2011; Schmittner et al. 2011) and under conditions prescribed by observations (Zhang et al 2015, 2017).

3 Results

3.1 Interannual variations of the April–May precipitation over the ICP

3.1.1 Precipitation in April and May

Figure 1a presents the monthly averaged mean surface air temperature and precipitation during the period of 1981–2016. The results show that the warmest months is in May, reaching over 27.2 °C. The monthly mean precipitation is strongly associated with the summer monsoon variability, which reveals that nearly 80% of total annual precipitation over the ICP occurs in the rainy season (May–October). Furthermore, it is also clearly shown in Fig. 1b that the monthly mean precipitation in April and May is highly correlated with the Oceanic Niño Index (ONI) in winter [D (-1) JF] and spring (MAM).

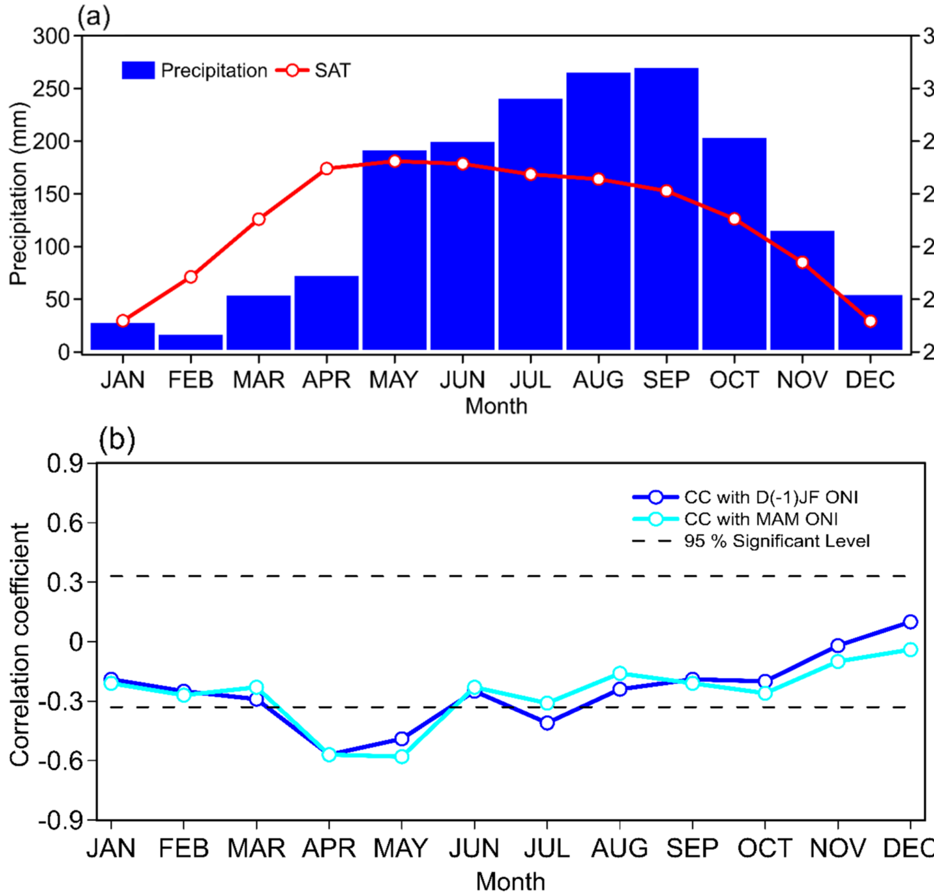

Fig. 1 **a** Monthly surface air temperature (SAT, red line, °C) and precipitation (blue bars, mm month $^{-1}$) during 1981–2016 over the ICP. **b** Correlation coefficients between monthly precipitation and the Oceanic Niño Index (ONI) in D (-1) JF (blue line) and MAM (cyan line). The black dash lines represent the 95% significant level

The temporal and spatial features of April and May (AM) precipitation over the ICP is explored by EOF analysis on the SA-OBS dataset. The first leading mode shows a uniform monopole pattern, accounting for 60% of the total variance (Fig. 2a). The linear correlation coefficients between the ONI and the normalized principal component of the first EOF mode (PC-1) are − 0.60 (Fig. 2b) and − 0.65 (Fig. 2c) in winter and spring, respectively, both passing the 95% significance level. In contrast, its correlation with the Indian Ocean dipole (IOD) index is only − 0.16 (not shown), which suggests that the AM precipitation is more closely related to SST anomalies of the Niño-3.4 region than to the IOD. The annual cycle of precipitation over Southeast Asia varies significantly due to the complex land-sea interaction associated with the reversed surface monsoonal winds. The southern part of ICP (e.g. Vietnam) and Malay Peninsula are influenced by the winter monsoon regime during boreal autumn and winter, and these rainfall events are also associated with the ENSO cycle (Chang et al. 2004, 2005; Zhou et al. 2008; Feng et al. 2010). In this study, we mainly focus on the precipitation anomalies over the ICP during the summer monsoon transition period represented by the wetter/drier than normal years of AM precipitation.

3.1.2 Relationship with SSTA

To investigate the year-to-year variability of AM precipitation over the ICP and its association with the SSTA patterns over tropical ocean, we categorize the normalized PC-1 from 1981 to 2016 with ± 1 std as the threshold, and obtain four wet years (1999, 2000, 2009, and 2011) and seven dry years (1983, 1987, 1992, 2005, 2014, 2015 and 2016), which are used for composite studies (Fig. 3a, b).

The BoBSM also plays an important role for the interannual variability of AM precipitation over the ICP. The dry years are usually concurrent with a late onset and a wet year with an early onset of the BoBSM. The selected dry and wet years are identical to the late and early BoBSM onset years (Fig. 3c). Note that SSTA composites in winter and spring closely resemble the El Niño (La Niña) pattern during dry (wet) years (Fig. 4), which are consistent with the results of previous studies (Liu et al. 2013; Nguyen-Le et al 2015; Xing et al. 2016; Li et al. 2018). They found that the composite SSTA over the western and central-eastern Pacific for

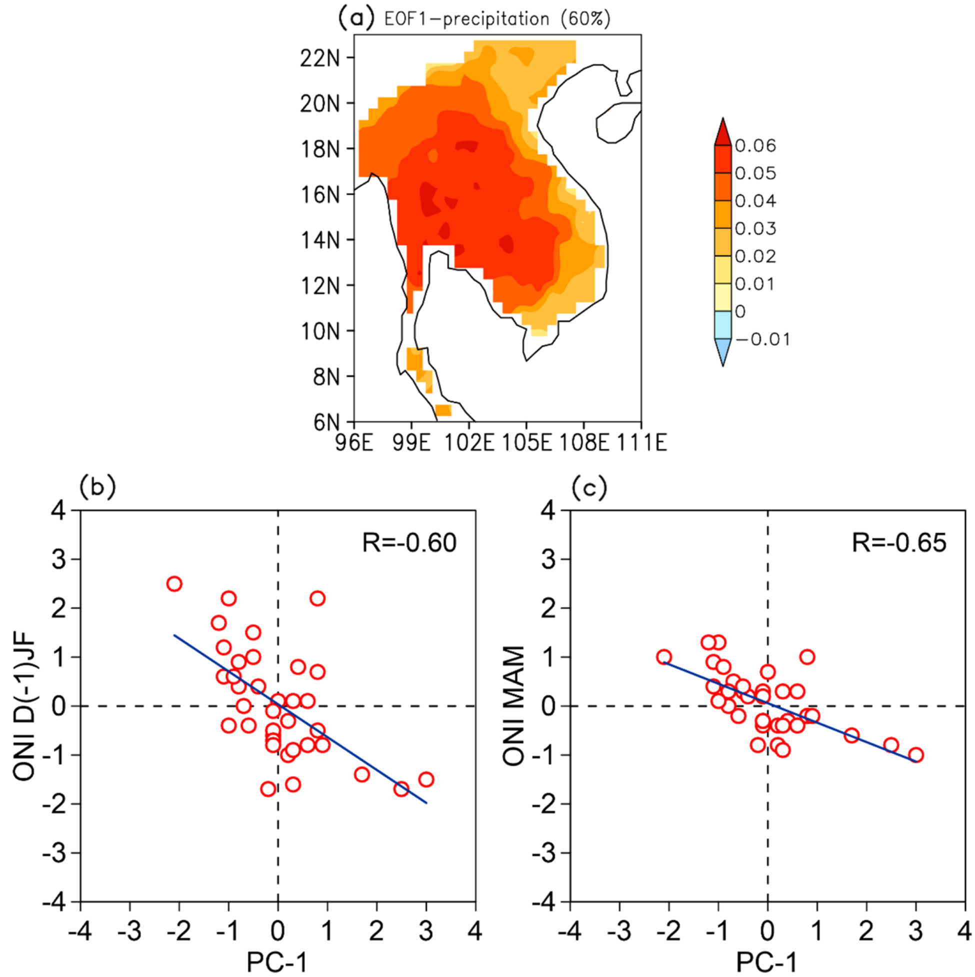

Fig. 2 **a** The first EOF mode of April–May (AM) precipitation during 1981–2016 over the ICP. **b** Scatterplots of the Oceanic Niño Index (ONI) and the normalized principal component of PC-1 in D (-1) JF. **c** Same as (**b**), but for MAM

early /late monsoon onset shows a typical ENSO pattern during the preceding winter and spring. In summarizing, ENSO events appear to modulate the AM precipitation anomalies, which are closely linked with the early /late BoBSM onset years. This modulating mechanism needs to be more deeply elucidated by analyzing the large-scale atmospheric circulation response to tropical SSTA and moisture transport during the dry and wet years in the following subsection.

3.2 Anomalous atmospheric circulation response to tropical SST forcing

3.2.1 Tropical atmospheric circulation

Wind field composites (Fig. 5a, b, arrows) of dry (wet) years are characterized by two anti-cyclonic (cyclonic) circulation anomalies over the BoB and WNP. The low-level atmospheric circulations are similar to those of early (late) BoBSM onset years over the ICP. Compared with its climatological mean conditions, the ICP is dominated by enhanced moisture divergence (convergence) anomalies (Fig. 5c, d, shaded areas) associated with the anomalous anti-cyclonic (cyclonic) flow during the dry (wet) years.

Actually, the direct atmospheric response to the equatorial central Pacific warming can be interpreted by the classical Matsuno-Gill response theory (Matsuno 1966; Gill 1980). That is, a pair of anomalous cyclonic circulations located along both sides of the equator and associated with the equatorial westerly anomalies. Formation and persistence of anti-cyclonic (cyclonic) circulation anomalies over the WNP, in terms of the Matsuno-Gill dynamics, is a Rossby wave response of the suppressed (enhanced) convective heating, which is induced by the local WNP SSTA cooling (warming) associated with the central-eastern Pacific warming (cooling). This Pacific-East Asian teleconnection could significantly influence the interannual variations of precipitation over the East and Southeast Asian (Wang et al 2000) and our observational results indeed support the theory.

During the dry years (Fig. 5a), the cold SSTA of the Maritime Continent (MC) favors the anomalous anti-cyclone. The returning southwesterly along the western flank of the WNP anti-cyclone dominates the ICP, thereby cutting Pacific moisture transports from the WNP into this region.

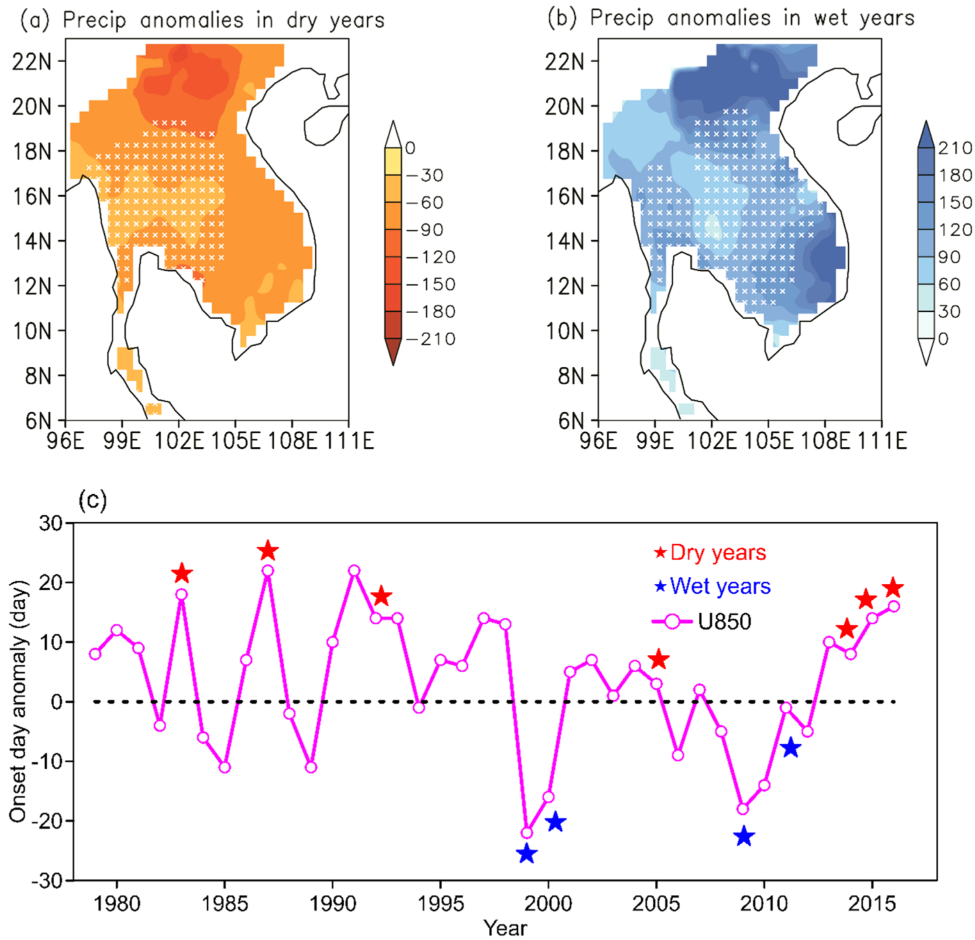

Fig. 3 Composites of precipitation anomalies (mm month $^{-1}$) in April–May (AM) during the dry (**a**) and wet (**b**) years. The white crosses indicate statistical significance at the 90% confidence level. **c** Time series of the BoBSM onset day anomalies defined by *U850*, the red and blue stars represent the dry and wet years, respectively

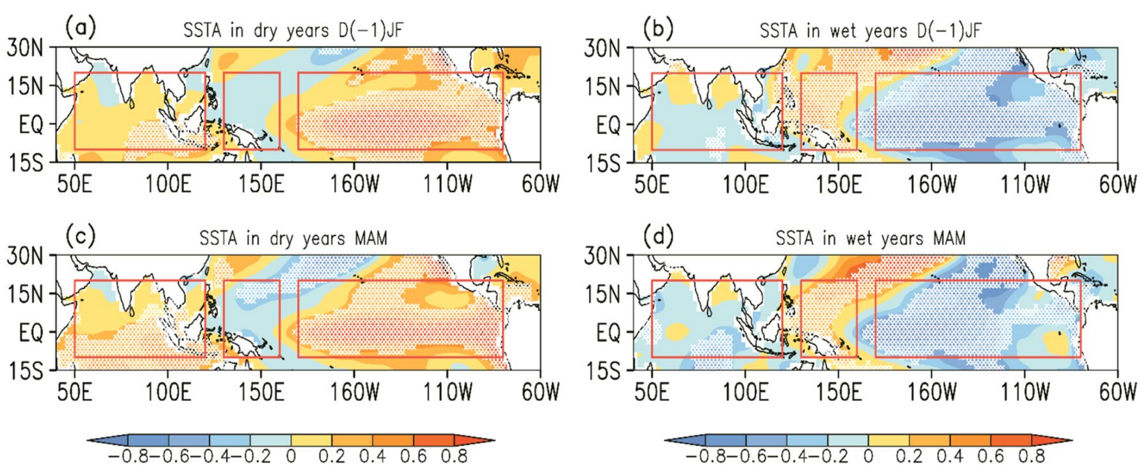

Fig. 4 Composites of SST anomalies (SSTA) in D (− 1) JF and MAM during dry (**a**, **c**) and wet (**b**, **d**) years. The white crosses indicate statistical significance at the 90% confidence level. The red rectangles represent three SSTA key areas

On the other hand, during the wet years (Fig. 5b), the situation is reversed due to La Niña conditions and the anomalous WNP cyclone being maintained.

The anti-cyclonic (cyclonic) circulation anomalies over the BoB, however, cannot be satisfactorily explained by a direct SST heating response mechanism as in the Matsuno-Gill model. It is noteworthy that the weaker positive SSTA has been found over the BoB during the dry year (Fig. 4c). That means, the local SST is warmer than the climatological mean and the anti-cyclone over the BoB (Fig. 5a) is not

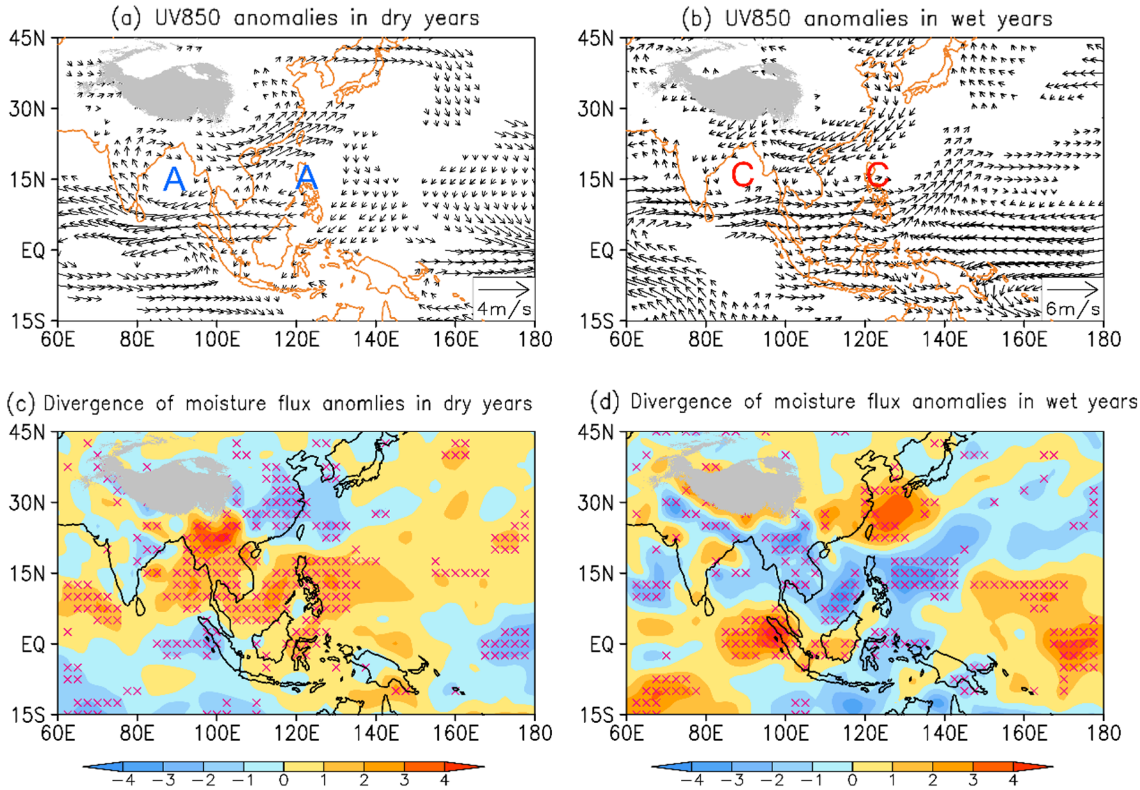

Fig. 5 Composites 850 hPa wind field anomalies (arrows, m/s) and vertical integral of divergence of moisture flux anomalies (shaded, 10^{-5} kg m^{-2} s^{-1}) in April–May (AM) during dry (**a**, **c**) and wet (**b**, **d**) years. Only anomalies statistically significant at the 90% confidence level for wind are shown in (**a**) and (**b**). Divergences of moisture flux are significantly stippled in purple crosses in (**c**) and (**d**). The marks of "A" and "C" indicate the centers of anomalous anti-cyclones and cyclones, respectively

consistent with the simultaneous SSTA. During the wet years, negative SSTA occurs over most of the tropical IO but the SST over the BoB is still warmer and the anomalous cyclonic circulation appears in this region. This result implies that the local SSTA probably is not the clue which establishes the anti-cyclone (cyclone) over the BoB nor account for its variability.

Atmospheric diabatic heating appears as another predominant contributor to induce circulation anomalies. This is clearly indicated by the weakened convective activity (as documented by the OLR anomalies) spreading from the BoB to South China Sea during the dry years (Fig. 6a), while enhanced convective activities occur over the BoB and ICP during the wet years (Fig. 6b). In addition, the vertically integrated apparent heat source $<Q_1>$ features appear to support our notion. The negative $<Q_1>$ anomalies cover the BoB and ICP during the dry years (Fig. 6c), while the positive $<Q_1>$ anomalies primarily dominate from the BoB via central ICP to the South China Sea (SCS) during the wet years (Fig. 6d). The anti-cyclonic (cyclonic) circulation anomalies are related to anomalous diabatic heating associated with convective activities over the BoB during the dry (wet) years. Xing et al (2016) also found that the anomalous atmospheric heating associated with the late (early) BoBSM onset contributes to the generation of an anomalous anti-cyclone (cyclone) over the BoB, which further suppress (favor) the precipitation in May over the southern Indian peninsula, the ICP and the SCS.

Moisture transport is mainly dominated by winds at the low level such as the 850 hPa, which is shown in Fig. 5. Therefore, drought conditions over the ICP can be attributed to influences of the westerlies along the northern flank of an enhanced anti-cyclone over the BoB and the southerlies along the northwestern flank of an extended anti-cyclone over the WNP. The two anomalous anti-cyclonic circulations transport the moisture from the SCS to the southern China, inducing the suppressed convection and decreased precipitation over the ICP. On the other hand, during the wet years, the reversed pattern occurs over the ICP. The abnormal AM precipitation over the ICP can be explained by the anomalous northeasterlies along the northern flank of an extended WNP cyclone and the enhanced westerlies along the southern flank of BoB cyclone. The two cyclonic circulations steer the moisture transport from the WNP and BoB to the ICP in April and May and subsequently

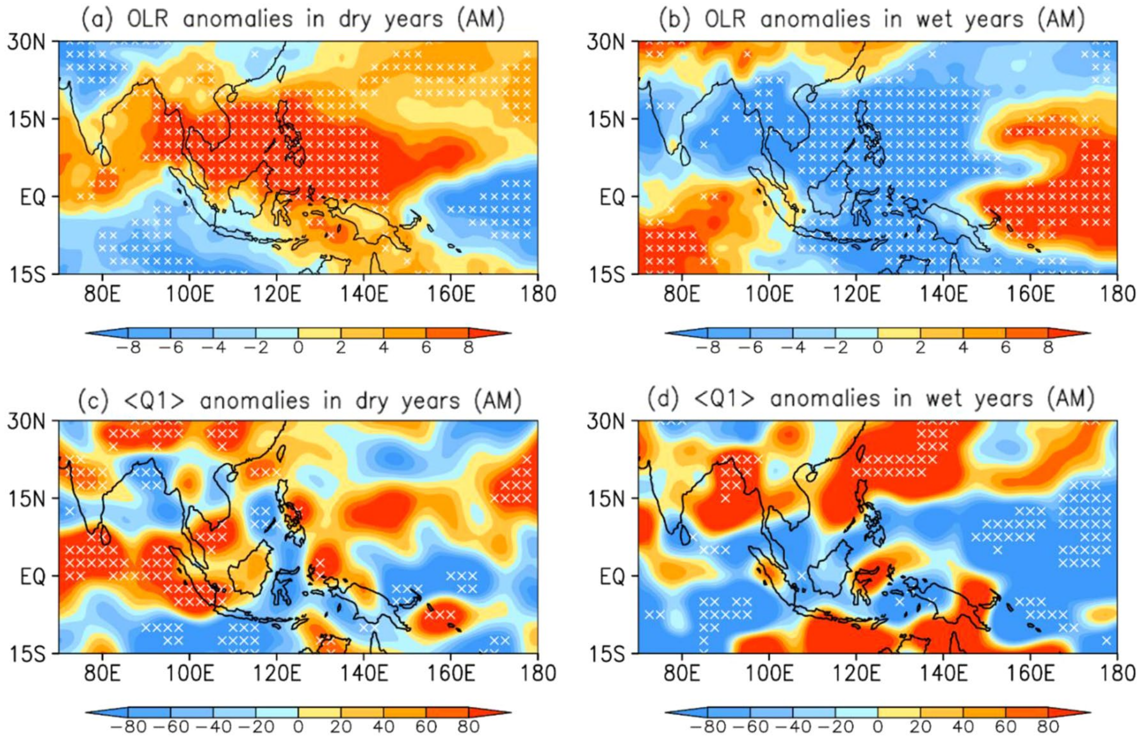

Fig. 6 Composites of OLR (**a**, **b**, W/m^2) and vertically integrated apparent heat source $<Q_1>$ (**c**, **d**, W/m^2) anomalies in April -May (AM) during dry and wet years. The white crosses indicate statistical significance at the 90% confidence level

increase the convergence inducing the larger than normal precipitation.

3.2.2 The role of Walker and Hadley circulation

Figure 7a–d shows the composite anomalies of the 850 and 200 hPa velocity potential and divergent wind during the dry and wet years. During the dry years, significant lower level convergences are observed over the tropical central-eastern Pacific, while the enhanced divergences appear over the WNP (Fig. 7a). Strong upper-level divergences predominately occur over the tropical central-eastern Pacific, whereas the anomalous convergences are located over the WNP (Fig. 7c). This implies that the eastward shifted/extended Walker circulation suppresses the convective activities over the MC and the anomalous heat sink excites the descending Rossby waves, which reinforce the anomalous anti-cyclone over the WNP during the dry years. In contrast, the wet years show the western Pacific being dominated by a lower-level center of convergence while strong divergence is observed over the tropical central-eastern Pacific (Fig. 7b). The reversed features can be found in the upper-level (Fig. 7d). These baroclinic patterns being linked with the SST anomalies over the tropical Pacific (Fig. 4), suggest that the SST anomalies associated with El Niño (La Niña) events appear to be driving the Walker circulation anomalies of opposite sign during dry and wet years.

The composite of mass streamfunction (MSF) anomalies over 115°–125°E are presented in Fig. 7e, f (Buja 1994; Nguyen et al 2013). This MSF streamfunction ($\Psi(p, y)$) is computed by vertically integrating the monthly meridional wind

$$\Psi(p, y) = \frac{2\pi a\cos(y)}{g} \int_{p}^{P_s} V(p, y)dp$$

where p is the pressure, y is the latitude, a is the average radius of Earth, g is the gravitational acceleration and P_s is the surface pressure. In the dry years, a weaker than normal local Hadley circulation is observed, while a stronger than normal local Hadley circulation appears in the wet years. This is consistent with the changes of Walker circulation, as revealed by the composite of lower–upper level velocity potential and divergence wind. The weaker local Hadley circulation in dry years, which is concurrent with the overturning Walker circulation, implies a weakened tropical convective activity (as documented by the OLR in Fig. 6a, b) over the MC and the ICP, which leads to a further decrease of precipitation in this region. The opposite holds for the wet years. These results suggest that changes of local Hadley circulation and Walker circulation appear to be responsible

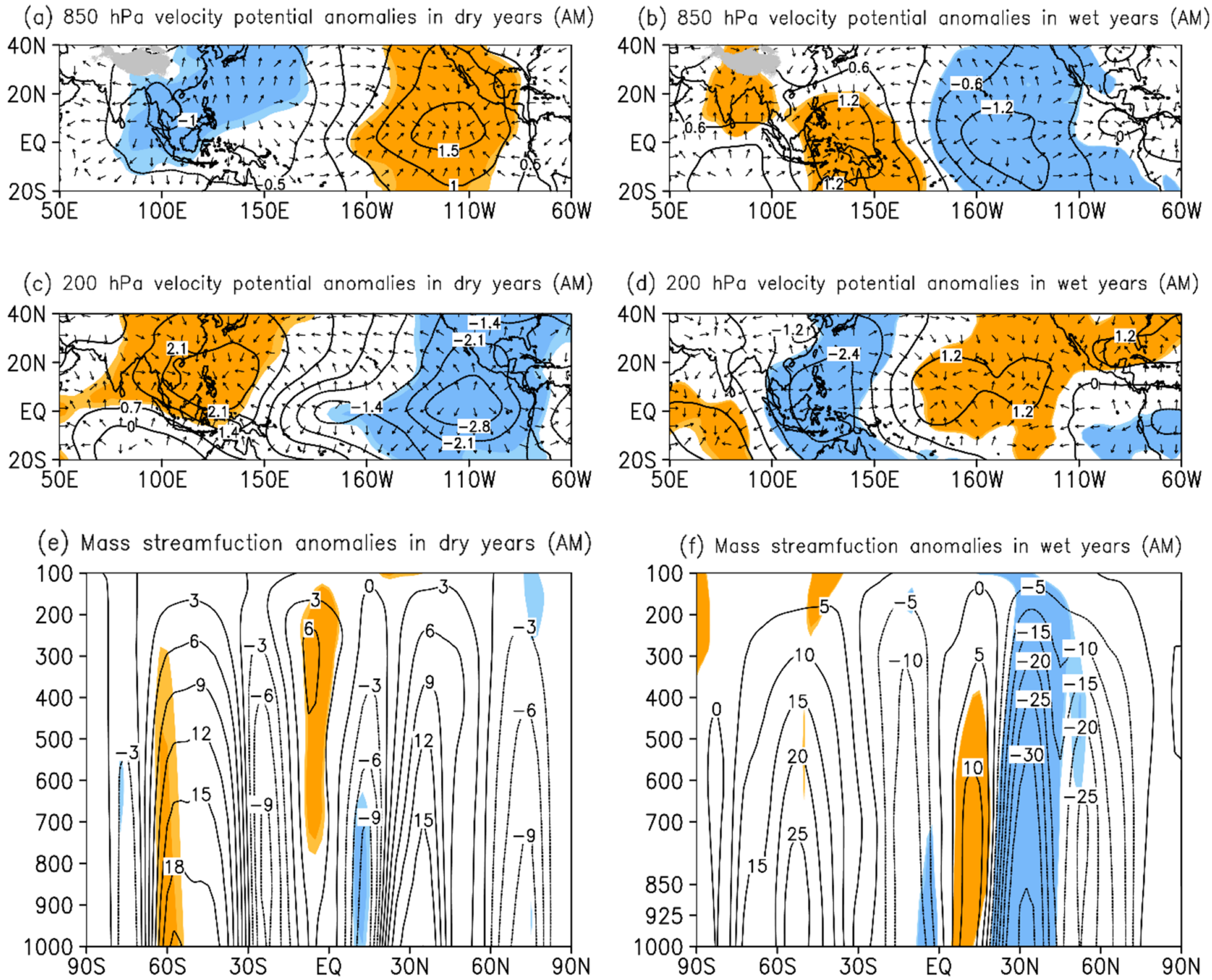

Fig. 7 850 and 200 hPa velocity potential (**a**–**d**, contours, 10^{-6} m^2/s), divergence wind (**a**–**d**, vectors, m/s) anomalies and cross sections of the mass streamfunction anomalies (**e**, **f**, 10^{10} kg/s) in April–May (AM) during dry and wet years, averaged over 115°–125°E. Shaded areas are statistically significant at the 90% confidence level

Table 1 Design of the PlaSim experiments

Experiment name	Experiment design
CTL	Control run with AMIP climatological SST
DRY	Winter and spring upscaled SSTA forcing in dry years over the tropics (Fig. 4a, c, red rectangles)
WET	Winter and spring upscaled SSTA forcing in wet years over the tropics (Fig. 4b, d, red rectangles)

for regulating the AM precipitation variability over the ICP. Note, that the Walker circulation links to ENSO SST anomalies, whereas the local Hadley circulation is attached to local meridional SST anomalies over the MC region.

In conclusion, the atmospheric circulation response to the tropical SSTA forcing is crucial for modulating the interannual variabilities of AM precipitation over the ICP. To verify the observed teleconnections between the tropical SSTAs and AM precipitation over the ICP, global circulation model experiments are performed with PlaSim-GCM in the following subsection.

4 Model experiments

4.1 Upscaled SSTA forcing

The climate mean control (CTL) case is compared with two sensitivity experiments with prescribed forcing by the observed tropical SST fields (Table1). The SST forcing of the CTL run is provided by the SST with annual cycle from the climatological global Atmospheric Model Intercomparison Project (AMIP). The control case is obtained from the last 20 years of the 30-year PlaSim control run. Analogously, the PlaSim sensitivity experiments are also integrated for 30 years with the results of last 20 years being used to construct a 20-ensemble member for investigating the simulated atmospheric response to the SSTA forcing. The SSTA are derived from the composites of seasonal mean SSTA over the key tropical areas in dry and wet years (Fig. 4, red rectangle). In order to obtain better atmospheric responses, we

Table 2 The averaged SSTA (°C) of the three key tropical areas and its corresponding upscaled SSTA (°C) imposed in the sensitivity experiments. The upscaled SSTA (°C) is highlighted in bold

SSTA key areas	Dry years		Wet Years	
	D (-1) JF	MAM	D (-1) JF	MAM
IO + MC (10°S–20°N,50°–120°E)	0.11 (**0.22**)	0.21 (**0.43**)	− 0.04 (**− 0.07**)	− 0.12 (**− 0.20**)
Western PAC (10°S–20°N,130°–160°E)	− 0.06 (**− 0.12**)	− 0.12 (**− 0.25**)	0.24 (**0.40**)	0.25 (**0.42**)
Central-Eastern PAC (10°S–20°N,180°–280°E)	0.47 (**0.96**)	0.49 (**1.00**)	−0.60 (**-1.00**)	−0.45 (**-0.75**)

IO: Indian ocean, MC: Maritime Continent, PAC: Pacific

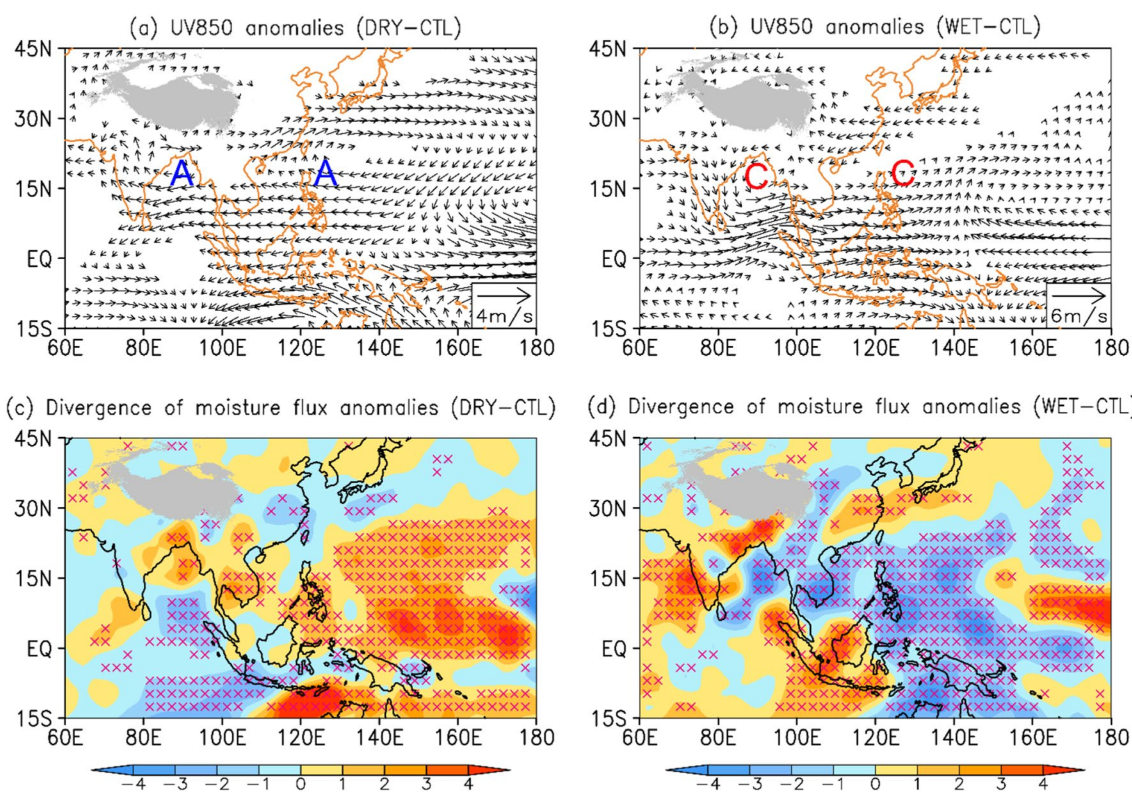

Fig. 8 Differences of 850 hPa wind field (arrows, m/s) and vertical integral of divergence of moisture flux (shaded, 10^{-5} kg m^{-2} s^{-1}) between two experiments in April–May (AM). **a**, **c** DRY-CTL, (**b**, **d**) WET-CTL. Only anomalies statistically significant at the 90% confidence level for wind are shown in (**a**) and (**b**). Divergences of moisture flux are significantly stippled in purple crosses in (c) and (d). The marks of "A" and "C" indicate the centers of anomalous anti-cyclones and cyclones, respectively

use the three area-averaged SSTAs, each for one of the three key tropical areas. It takes better into account the different spatial variances of the SSTA forcing areas than only using the spatial means since the three key tropical regions are highly related in the dry and wet year cases. These are upscaled based on the formula:

$$\mathrm{SSTA}_{upscaled} = \mathrm{SSTA} \times \frac{1}{\mathrm{SSTA}_{max}}$$

with SSTA_{max} as the maximum within the forcing area (red rectangle). The averaged SSTA of the three key tropical areas and its corresponding upscaled SSTAs are listed in Table 2.

4.2 GCM responses

The simulated atmospheric circulation and moisture transport responses to the abnormal SST forcing of the tropical ocean during dry and wet years are shown in Fig. 8a and b (after subtracting CTL runs from sensitivity experiments). Compared with the observed circulation composites (Fig. 5a, b) the 850 hPa wind and moisture responses are well reproduced by PlaSim. In the DRY-experiment, the anomalous lower-level anti-cyclone occurs over the WNP with a slight eastward extension, while the abnormal anti-cyclone appears over the BoB with reduced meridional extent. The southwesterlies caused by the anti-cyclone over the WNP transports abundant moisture to South China and the northwesterlies associated with the BoB anti-cyclone brings more dry air from the Indian subcontinent, leading to drought conditions over the ICP (Fig. 8a). By contrast, in the WET-experiment, two anomalous low-level cyclonic circulation centers occur over the BoB and WNP, with enhanced moisture convergence over the ICP (Fig. 8b).

In summarizing, the SSTA forcing experiments confirm the modulating mechanisms analyzed in Sect. 3, which explain the observed remote impacts of the tropical SSTAs on the interannual variability of AM precipitation observed over the ICP.

5 Conclusions and discussion

The interannual variability of April–May (AM) precipitation over the Indochina Peninsula (ICP) has been investigated for the time period 1981–2016 using observed monthly precipitation data. The analysis of the large-scale atmospheric response to tropical SSTA is based on reanalysis data and results from experiments with Planet Simulator (PlaSim), a climate model of intermediate complexity. The results are comprised in a schematic diagram (Fig. 9) and illustrated as follows.

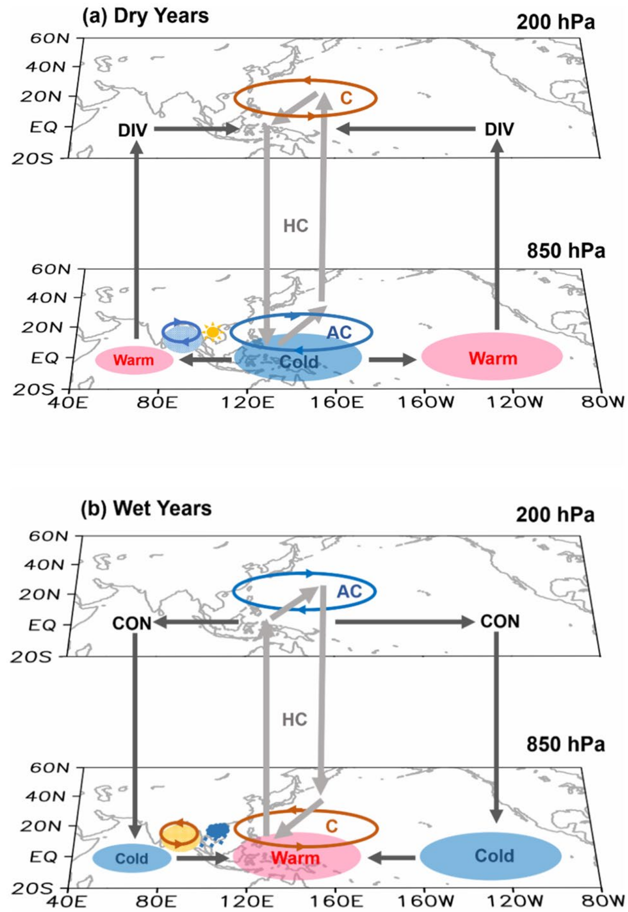

Fig. 9 Schematic diagram of atmospheric circulation anomalies in lower level (850 hPa) and upper level (200 hPa) during dry and wet years. Red/blue shaded areas indicate warm/cold SST anomalies. Light blue/yellow shaded areas over the BoB represent the diabatic heating < Q_1 > anomalies. *AC/C* represents the anomalous anti-cyclone/cyclone. Black and grey arrows indicate anomalous zonal and meridional circulation branches, respectively. *CON and DIV* indicate convergence and divergence at the upper level. *HC* represents the anomalous Hadley Circulation

(i) The climatological monthly mean precipitation in AM over the ICP are highly correlated with the preceding winter [D (-1) JF] and spring (MAM) SSTA over the central-eastern Pacific. There is a close relationship between the dry/wet conditions over the ICP and the ENSO phenomenon. The below (above) normal AM precipitation over the ICP coincides with El Niño (La Niña) years, which also corresponds well to the late (early) BoBSM onset years. The atmospheric circulation response to the tropical SSTA forcing plays an important role on interannual variability of AM precipitation over the ICP.

(ii) During the dry years, the anomalous WNP anti-cyclone induced by El Niño, transports abundant moisture to South China by enhanced southwesterlies, while the anti-cyclone over the BoB brings cold and dry air from Indian subcontinent to the ICP. The reduced tropical convective activities occur over the MC and the ICP due to the weakened local Hadley circulation concurrent with the overturning Walker circulation, which favor drier than normal conditions over the ICP (Fig. 9a).

(iii) During the wet years, the northeasterly anomalies along the northwestern flank of WNP cyclone bring more moisture from Pacific to the ICP, while cyclonic circulation over the BoB also transports abundant warm and humid air to the ICP. The strengthened local Hadley circulation concurrent with the enhanced Walker circulation indicate more tropical convective activities over the MC and the ICP, which leads to a wetter than normal conditions (Fig. 9b).

The sensitivity experiments conducted with PlaSim successfully reproduce the teleconnections between the AM precipitation over the ICP and the tropical SSTA forcing, which further confirms the modulating mechanism explaining the prolonged atmospheric responses to ENSO events.

Located in Southeast Asia, the ICP is presently attracting increasing concern due to its high climate risk exposure to global warming. A comprehensive understanding of the year-to-year variability of temperature and precipitation is of critical importance to mitigate the potential threat for the developing countries of the ICP. More work remains necessary to be conducted on comparisons of the moisture supply in present and future climate over this region (Li et al. 2013; Li and Zhou 2016). It is evident that the ongoing global warming has enhanced severe extremes during the past two decades, which makes the ecosystem vulnerable and becoming more fragile in this region (IPCC 2018; Eckstein et al. 2019). This is a condition, which is very likely to continue into the not too distant future. Thirumalai et al. (2017) have shown that the robust relationship between ENSO and the SATs in Southeast Asia, especially all April temperature extremes over the ICP, have occurred during El Niño years. Yang and Wu (2019) found that the variations of March–April precipitation over the ICP are significantly influenced by the increasing thermal contrast between the neighboring SST and atmospheric column, which is modulated by the surface heat fluxes changes.

In addition, the SCS and IO also play important roles in precipitation anomalies over the surrounding areas of the ICP (e.g. southern China and MC). The eastward WNP anti-cyclone induced by canonical El Niño enhances meridional moisture transport from the SCS, which results in an increased precipitation over Southern China. On the other hand, the westward shift of WNP anti-cyclone associated with the El Niño Modoki suppresses the meridional moisture transport from the SCS, leading to a decreased precipitation over Southern China (Wang et al. 2018, 2019). Abnormal moisture transport can generate higher sea surface salinity over the SCS, which further influences the summer precipitation over the middle and lower Yangtze River Valley of China (Zeng et al. 2019). Positive (negative) SSTAs over the tropical western IO could induce a suppressed (enhanced) Walker circulation over the tropical IO and WNP, leading to a weaker (stronger) monsoon trough in the SCS, which further reduces (increases) precipitation in June over the ICP (Leung et al. 2020). The abnormal positive IOD event during 2015/2016 could establish the El Niño-SCS connection in August, which leads to an early anomalous anticyclone (AAC) and further suppresses the rainfall over the MC and ICP (Xiao et al. 2020).

More recently, Ge et al. (2019) and Zhu et al. (2020b) have pointed out the impacts of global warming on climatic stresses in Southeast Asia especially in the densely populated large coastal regions of the ICP and have further revealed the necessity of restricting the warming trends. In any case, the record-breaking droughts and floods, super ENSO events, and intensified tropical cyclones make the detection and attribution of climate change even more challenging in the tropics. In addition to the underlying impacts of the tropical SSTAs shown in this study, these results suggest to further analyze the climate conditions of Southeast Asia mainland and to initiate wider attention to this region, in order to support sustainable future development.

Acknowledgements Anonymous reviewers are thanked for their constructive comments that greatly improved the quality of the manuscript. We are grateful to Dr. Andrea Schneidereit, Dr. Frank Lunkeit and Prof. Yuanfa Gong for inspiring discussions on the PlaSim experiments and the anomalous atmospheric circulation patterns. We would like to thank the German Climate Computing Center (DKRZ) for their resources.

Funding The National Natural Science Foundation of China (Grant Nos 41805056 and U20A2097), the Application and Basic Research of Sichuan Department of Science and Technology (2019YJ0316), the Special Funds for the Central Government to Guide Local Technological Development (2020ZYD051).

References

Allen MR, Ingram WJ (2002) Constraints on future changes in climate and the hydrologic cycle. Nature 419:224–228

Bordi I, Fraedrich K, Sutera A, Zhu X (2012) On the climate response to zero ozone. Theor Appl Climatol 109:253–259

Bordi I, Fraedrich K, Sutera A, Zhu X (2013) On the effect of decreasing CO_2 concentration in the atmosphere. Clim Dyn 40:651–662

Buja LE (1994) CCM processor user's guide (Unicos version). NCAR Tech. Note NCAR/TN-3841IA, 250 pp

Caesar J, Alexander LV, Trewin B (2011) Changes in temperature and precipitation extremes over the Indo-Pacific region from 1971 to 2005. Int J Climatol 31:791–801
Chang CP, Harr PA, McBride J, Hsu HH (2004) Maritime Continent monsoon. In: Chang CP (ed) East Asian Monsoon. World Scientific Publishing, Singapore, pp 107–150
Chang CP, Wang Z, McBride J, Liu C (2005) Annual cycle of Southeast Asia-Maritime continent rainfall and the asymmetric monsoon transition. J Clim 18:287–301
Dahms E, Borth H, Lunkeit F, Fraedrich K (2011) ITCZ splitting and the influence of large-scale eddy fields on the tropical mean state. J Meterol Soc Jpn 89(5):399–411
Eckstein D, Künzel V, Schäfer L (2019) Global climate risk index 2019. Germanwatch Available online: https://germanwatch.org/en/16046
Fan Y, Fan K, Xu Z, Li S (2018) ENSO–South China Sea summer monsoon interaction modulated by the Atlantic Multidecadal Oscillation. J Clim 31:3061–3076
Fan Y, Fan K, Zhu X, Fraedrich K (2019) El Niño-related summer precipitation anomalies in Southeast Asia modulated by the Atlantic multidecadal oscillation. J Clim 32:7971–7987
Feng J, Wang L, Chen W, Fong SK, Leong KC (2010) Different impacts of two types of Pacific Ocean warming on Southeast Asian rainfall during boreal winter. J Geophys Res 115:D24122
Fraedrich K, Jansen H, Kirk E, Luksch U, Lunkeit F (2005a) The planet simulator: towards a user friendly model. Meteorol Z 14:299–304
Fraedrich K, Kirk E, Luksch U, Lunkeit F (2005b) The portable university model of the atmosphere (PUMA): Storm track dynamics and low-frequency variability. Meteorol Z 14:735–745
Fudeyasu H, Iizuka S, Matsuura T (2006) Seasonality of westward-propagating disturbances over Southeast and south Asia originated from typhoons. Geophys Res Lett 33:L10809
Ge F, Zhu S, Peng T et al (2019) Risks of precipitation extremes over Southeast Asia: does 1.5 °C or 2 °C global warming make a difference? Environ Res Lett 14:044015
Ge F, Zhi X, Babar ZA, Tang W, Chen P (2017) Interannual variability of summer monsoon precipitation over the Indochina Peninsula in association with ENSO. Theor Appl Climatol 128:523–531
Ge F, Zhu S, Luo H, Zhi X, Wang H (2021) Future changes in precipitation extremes over Southeast Asia: insights from CMIP6 multi-model ensemble. Environ Res Lett 16:024013
Gill AE (1980) Some simple solutions for heat-induced tropical circulation. Quart J Roy Meteor Soc 106:447–462
He J, Zhu Z (2015) The relation of South China Sea monsoon onset with the subsequent rainfall over the subtropical East Asia. Int J Climatol 35:4547–4556
He H, McGinnis JW, Song Z, Yanai M (1987) Onset of the Asian summer monsoon in 1979 and the effect of the Tibetan Plateau. Monthly Weather Rev 115:1966–1994
Holden PB, Edwards NR, Garthwaite PH, Fraedrich K, Lunkeit F, Kirk E, Labriet M, Kanudia A, Babonneau F (2014) PLASIM-ENTSem v1.0: a spatio-temporal emulator of future climate change for impacts assessment. Geosci Model Dev 7:433–451
Holden PB, Edwards NR, Fraedrich K, Kirk E, Lunkeit F, Zhu X (2016) PLASIM-GENIE: a new intermediate complexity AOGCM. Geosci Model Dev 9:3347–3361
Hsu HH, Zhou T, Matsumoto J (2014) East Asian, Indochina and western North Pacific summer monsoon-an update. Asia-Pac J Atmos Sci 50(1):45–68
Huang B, Coauthors (2015) Extended Reconstructed Sea Surface Temperature version 4 (ERSST.v4): Part I Upgrades and Intercomparisons. J Clim 28:911–930
Huang B, Thorne PW, Banzon VF, Boyer T, Chepurin G, Lawrimore JH, Zhang HM (2017) Extended reconstructed sea surface temperature, version 5 (ERSSTv5): upgrades, validations, and intercomparisons. J Clim 30:8179–8205
IPCC (2018) Global Warming of 1.5 ºC, an IPCC special report on the impacts of global warming of 1.5ºC above pre-industrial levels and related global greenhouse gas emission pathways, in the context of strengthening the global response to the threat of climate change, sustainable development, and efforts to eradicate poverty. World Meteorological Organization, Geneva
Kalnay E, Kanamitsu M, Kistler R, Collins W, Deaven D, Gandin L, Zhu Y (1996) The NCEP/NCAR 40-year reanalysis project. Bull Am Meteorol Soc 77:437–471
Knutson TR, Coauthors, (2010) Tropical cyclones and climate change. Nat Geosci 3:157–163
Lau KM, Yang S (1997) Climatology and interannual variability of the southeast Asian summer monsoon. Adv Atmos Sci 14:141–162
Lau KM, Kim KM, Yang S (2000) Dynamical and boundary forcing characteristics of regional components of the Asian summer monsoon. J Clim 13:2461–2482
Leung MY-T, Zhou W, Wang D, Chan PW, Lee SM, Tong HW (2020) Remote tropical western Indian Ocean forcing on changes in June precipitation in South China and the Indochina Peninsular. J Clim 33:7553–7566
Li JP, Zhang L (2009) Wind onset and withdrawal of Asian summer monsoon and their simulated performance in AMIP models. Clim Dyn 32:935–968
Li XZ, Zhou W (2016) Modulation of the interannual variation of the India-Burma Trough on the winter moisture supply over Southwest China. Clim Dyn 46:147–158
Li XZ, Zhou W, Li CY, Song J (2013) Comparison of the annual cycles of moisture supply over Southwest and Southeast China. J Clim 26(10139–10):158
Li KP, Liu Y, Li Z, Yang Y, Feng L, Khokiattiwong S, Yu W, Liu S (2018) Impacts of ENSO on the Bay of Bengal summer monsoon onset via modulating the intraseasonal oscillation. Geophys Res Lett 45:5220–5228
Liebmann B, Smith CA (1996) Description of a complete (interpolated) outgoing longwave radiation dataset. Bull Am Meteorol Soc 77:1275–1277
Liu B, Wu G, Mao J, He J (2013) Genesis of the South Asian high and its impact on the Asian summer monsoon onset. J Clim 26:2976–2991
Liu B, Liu Y, Wu G, Yan J, He J, Ren S (2015) Asian summer monsoon onset barrier and its formation mechanism. Clim Dyn 45:711–726
Lunkeit F, Borth H, Böttinger M, Fraedrich K, Jansen H, Kirk E, Kleidon A, Luksch U, Paiewonsky P, Schubert S, Sielmann F, Wan H (2011) Planet simulator reference manual version 16. Universität Hamburg, Meteorologisches Institut
Manton MJ, Della-Marta PM, Haylock MR et al (2001) Trends in extreme daily rainfall and temperature in Southeast Asia and the South Pacific: 1961–1998. Int J Climatol 21:269–284
Mao J, Wu G (2007) Interannual variability in the onset of the summer monsoon over the eastern Bay of Bengal. Theor Appl Climatol 89(3–4):155–170
Matsumoto J (1992) The seasonal changes in Asian and Australian monsoon regions. J Meteor Soc Jpn 70:15–32
Matsumoto J (1997) Seasonal transition of summer rainy season over Indochina and adjacent monsoon region. Adv Atmos Sci 14(2):231–245
Matsuno T (1966) Quasi-geostrophic motions in the equatorial area. J Meteor Soc Jpn 44:25–43
McBride JL, Haylock MR, Nicholls N (2003) Relationships between the Maritime Continent heat source and the El Niño-Southern Oscillation phenomenon. J Clim 16:2905–2914

Nguyen H, Evans A, Lucas C, Smith I, Timbal B (2013) The Hadley circulation in reanalyses: climatology, variability, and change. J Clim 26:3357–3376
Nguyen DQ, Renwick J, McGregor J (2014) Variations of surface temperature and rainfall in Vietnam from 1971 to 2010. Int J Climatol 34(1):249–264
Nguyen-Le D, Matsumoto J, Ngo-Duc T (2015) Onset of the rainy season in the eastern Indochina Peninsula. J Clim 28:5645–5666
Nicholls N, Baek HJ, Gosai A et al (2005) The El Niño-Southern Oscillation and daily temperature extremes in east Asia and the west Pacific. Geophys Res Lett 32:L16714
Schmittner A, Silva TA, Fraedrich K, Kirk E, Lunkeit F (2011) Effects of mountains and ice sheets on global ocean circulation. J Clim 24(11):2814–2829
Sein ZMM, Zhi X (2016) Interannual variability of summer monsoon rainfall over Myanmar. Arab J Geosci 9:469
Takahashi HG, Yasunari T (2006) A climatological monsoon break in rainfall over Indochina-A singularity in the seasonal march of the Asian summer monsoon. J Clim 19(8):1545–1556
Takahashi HG, Yasunari T (2008) Decreasing trend in rainfall over Indochina during the late summer monsoon: Impact of tropical cyclones. J Meteor Soc Jpn 86(3):429–438
Takahashi HG, Fujinami H, Yasunari T, Matsumoto J, Baimoung S (2015) Role of tropical cyclones along the monsoon trough in the 2011 Thai flood and interannual variability. J Clim 28:1465–1476
Thirumalai K, DiNezio PN, Okumura Y, Deser C (2017) Extreme temperatures in Southeast Asia caused by El Niño and worsened by global warming. Nat Commun 8:15531
Van den Besselaar EJ, Van der Schrier G, Cornes RC, Iqbal AS, Klein Tank AM (2017) SA-OBS: a daily gridded surface temperature and precipitation dataset for Southeast Asia. J Clim 30(14):5151–5165
Villafuerte MQ, Matsumoto J (2015) Significant influences of global mean temperature and ENSO on extreme rainfall in Southeast Asia. J Clim 28(5):1905–1919
Wang B, Chan JC (2002) How strong ENSO events affect tropical storm activity over the western North Pacific. J Clim 15(13):1643–1658
Wang B, Fan Z (1999) Choice of South Asian summer monsoon indices. Bull Am Meteor Soc 80(4):629–638
Wang B, LinHo (2002) Rainy season of the Asian–Pacific summer monsoon. J Clim 15:386–398
Wang B, Wu R, Fu X (2000) Pacific-East Asian teleconnection: How does ENSO affect East Asian climate? J Clim 13:1517–1536
Wang B, Wu R, Lau KM (2001) Interannual variability of the Asian summer monsoon: Contrasts between the Indian and the western North Pacific-East Asian monsoons. J Clim 14(20):4073–4090
Wang B, LinHo ZY, Lu M (2004) Definition of South China Sea monsoon onset and commencement of the East Asia summer monsoon. J Clim 17:699–710
Wang X, Jiang X, Yang S, Li Y (2013) Different impacts of the two types of El Niño on Asian summer monsoon onset. Environ Res Lett 8(4):575–591
Wang Q, Cai W, Zeng L, Wang D (2018) Nonlinear meridional moisture advection and the ENSO-southern China rainfall teleconnection. Geophys Res Lett 45:4353–4360
Wang Q, Cai W, Zhong W, Zeng L, Wu L, Wang D (2019) Response of southern China winter rainfall to El Niño diversity and its relevance to projected southern China rainfall change. J Clim 32:3343–3356
Webster PJ, Magana VO, Palmer TN, Shukla J, Tomas RA, Yanai MU, Yasunari T (1998) Monsoons: processes, predictability, and the prospects for prediction. J Geophys Res 103(C7):14451–14510
Wu R, Wang B (2000) Interannual variability of summer monsoon onset over the western North Pacific and the underlying processes. J Clim 13(14):2483–2501
Wu G, Zhang YS (1998) Tibetan Plateau forcing and the timing of the monsoon onset over South Asian and the South China Sea. Monthly Weather Rev 126:913–927
Xiao F, Wang D, Leung MYT (2020) Early and extreme warming in the South China Sea during 2015/2016: role of an unusual Indian Ocean Dipole event. Geophys Res Lett 47:e2020GL089936
Xing N, Li JP, Wang LN (2016) Effect of the early and late onset of summer monsoon over the Bay of Bengal on Asian precipitation in May. Clim Dyn 47:1961–1970
Yanai M, Li CF (1994) Mechanism of heating and the boundary layer over the Tibetan Plateau. Mon Wea Rev 122:305–323
Yanai M, Esbensen S, Chu JH (1973) Determination of bulk properties of tropical cloud clusters from large-scale heat and moisture budgets. J Atmos Sci 30(4):611–627
Yanai M, Li CF, Song ZS (1992) Seasonal heating of the Tibetan Plateau and its effects on the evolution of the Asian summer monsoon. J Meteor Soc Jpn 70:319–351
Yang Y, Wu R (2019) Seasonal variation of precipitation over the Indochina Peninsula and its impact on the South China Sea spring warming. Int J Climatol 35(3):1618–1633
Zeng L, Schmitt RW, Li L, Wang Q, Wang D (2019) Forecast of summer precipitation in the Yangtze River valley based on South China Sea springtime sea surface salinity. Clim Dyn 53:5495–5509
Zhang Y, Li T, Wang B, Wu G (2002) Onset of the summer monsoon over the Indochina Peninsula: Climatology and interannual variations. J Clim 15:3206–3221
Zhang W, Jin FF, Turner A (2014) Increasing autumn drought over southern China associated with ENSO regime shift. Geophys Res Lett 41:4020–4026
Zhang L, Sielmann F, Fraedrich K, Zhu X, Zhi X (2015) Variability of winter extreme precipitation in Southeast China: contributions of SST anomalies. Clim Dyn 45:2557–2570
Zhang L, Sielmann F, Fraedrich K, Zhi X (2017) Atmospheric response to Indian Ocean Dipole forcing: changes of Southeast China winter precipitation under global warming. Clim Dyn 48:1467–1482
Zhou T, Hsu HH, Matsuno J (2011) Summer monsoons in East Asia, Indochina and the Western North Pacific. The global monsoon system: Research and forecast, pp 43–72
Zhou T, Yu R, Li H, Wang B (2008) Ocean forcing to changes in global monsoon precipitation over the recent half-century. J Clim 21:3833–3852
Zhu Z (2018) Breakdown of the relationship between Australian summer rainfall and ENSO caused by tropical Indian Ocean SST warming. J Clim 31:2321–2336
Zhu S, Ge F, Fan Y et al (2020a) Conspicuous temperature extremes over Southeast Asia: seasonal variations under 1.5 °C and 2 °C global warming. Clim Change 160:343–360
Zhu S, Ge F, Sielmann F et al (2020b) Seasonal temperature response over the Indochina Peninsula to a worst-case high emission forcing: a study with the regionally coupled model ROM. Theor Appl Climatol 142:613–622